Anisotropic Absorption in PbSe Nanorods

Paul D. Cunningham,* Janice E. Boercker, Diogenes Placencia, and Joseph G. Tischler

U.S. Naval Research Laboratory, 4555 Overlook Avenue SW, Washington, D.C. 20375, United States

ABSTRACT We present absorption anisotropy measurements in PbSe nanostructures. This is accomplished *via* a new means of measuring absorption anisotropy in randomly oriented solution ensembles of nanostructures *via* pump–probe spectroscopy, which exploits the polarization memory effect. We observe isotropic absorption in nanocrystals and anisotropic absorption in nanorods, which increases upon elongation from aspect ratio 1 to 4 and is constant for longer nanorods. The measured volume-normalized absorption cross section is 1.8 ± 0.3 times larger for parallel pump and probe polarizations in randomly oriented nanorods as compared to nanocrystals. We show that this enhancement would be larger than an order of magnitude for aligned nanorods. Despite being in the strong quantum confinement regime, the aspect ratio dependence of the absorption anisotropy in PbSe nanorods is described classically by the effects of dielectric contrast on an anisotropic nanostructure. These results imply that the dielectric constant of the surrounding medium can be used to influence the optoelectronic properties of nanorods, including polarized absorption and emission, phonon modes, multiple exciton generation efficiency, and Auger recombination rate.

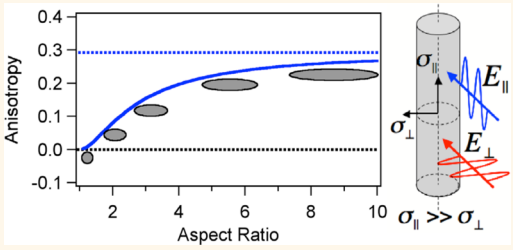

KEYWORDS: PbSe · nanorods · polarization memory · absorption · anisotropy · local field · dielectric contrast · Maxwell–Garnett

Colloidal semiconductor nanostructures are under intense research for a number of applications including next-generation solar cells,[1–5] photodetectors,[6] light-emitting diodes,[7,8] lasers,[9,10] and biological labeling.[11] Much of this work has centered on spherically symmetric nanocrystals due to their size-tunable band gap, large absorption cross sections, and sizable luminescent quantum yields. Among their optoelectronic properties multiple exciton generation (MEG) has been of particular interest over the past decade, as it provides a means to achieve charge carrier quantum yields larger than 100%.[2]

More recently, semiconducting nanorods and nanowires have been explored for these same applications. Elongation of these nanostructures provides a means of suppressing Auger recombination,[12,13] which limits many optoelectronic applications by introducing a rapid nonradiative decay route for multiple excitons. Furthermore, it is expected that charge carrier transport will be enhanced down the length of elongated nanostructures, which may yield improvements in photovoltaic or photodetector devices fabricated from these nanostructures. It has been recently shown that MEG is enhanced in elongated PbSe nanorods compared to nanocrystals,[14–16] with a tentative assignment to enhanced Coulombic interactions. This enhancement in Coulombic interactions was predicted for nanorods and wires due to reduced dielectric screening, as the electric field penetrates outside of the elongated nanostructure into the low dielectric external media.[17] The "dielectric contrast" between the dielectric constants of the nanostructure and external media gives rise to the reduced screening.

Dielectric contrast and the asymmetric shape of nanorods and wires also yield polarized light emission[18–20] and pronounced anisotropic absorption.[21] This has been confirmed in the case of CdSe nanowires by emission polarization memory measurements,[22,23] photocurrent measurements,[24] and single-wire extinction spectroscopy.[25] Very recently, transient absorption and photoluminescence excitation spectra anisotropy measurements have observed anisotropic absorption in CdSe nanorods.[26] Dielectric contrast also causes an enhancement of the oscillator strength and thus an increase in the absorption cross section in elongated nanostructures.[27]

* Address correspondence to paul.cunningham@nrl.navy.mil.

Received for review October 4, 2013 and accepted December 19, 2013.

Published online December 19, 2013
10.1021/nn405184j

© 2013 American Chemical Society

Recent MEG studies indicate an increase in the absorption cross section of PbSe nanorods compared to nanocrystals.[14,28] However, these measurements were on randomly oriented colloidal suspensions and do not account for the anisotropic nature of elongated nanostructures.

Here we exploit the so-called "polarization memory" effect in pump−probe spectroscopy in order to measure the absorption anisotropy of PbSe nanorods and nanocrystals. We observe anisotropic absorption in nanorods, while nanocrystals show isotropic absorption. Aspect ratio-dependent measurements show the evolution of the absorption properties for zero-dimensional to quasi-one-dimensional nanostructures. Our observations can be described classically by dielectric contrast between the nanostructures and the surrounding solvent, with no need for quantum confinement effects even though these nanorods have radii more than an order of magnitude smaller than the Bohr radius and are thus in the strong quantum confinement regime. The applicability of this classical model allows for estimation of the anisotropy and absorption cross sections of aligned nanorods. These results suggest that some optoelectronic properties of nanorods may be influenced by changing the dielectric properties of the surrounding medium.

RESULTS AND DISCUSSION

Absorption Cross-Section Measurement. We exploit the same methodology used to measure MEG quantum yields in colloidal nanostructures *via* pump−probe spectroscopy in order to measure the absorption cross section, but in this case with polarization-sensitive degenerate pump−probe spectroscopy at the band edge energy. Though photoexcitation occurs at the band edge energy, where MEG is forbidden by conservation of energy, sequential photon absorption at high fluences can lead to the creation of more than one exciton per nanostructure. If two or more excitons are present in a nanostructure, Auger recombination (AR) occurs on a time scale of ∼100 ps,[13] resulting in single excitons that recombine over 0.01−1 μs. We monitor the exciton dynamics by probing the sample at the ground state 1S absorption feature, *i.e.*, the band edge. Upon photoexcitation, the absorption of a pump photon creates an exciton, which bleaches the $1S_e-1S_h$ absorption feature due to state filling. The peak photoinduced bleach is proportional to the number of excitons created, which is proportional to the fluence, J_0. The magnitude of the bleach observed at long delays after AR is complete, *i.e.*, ∼1 ns, is proportional to the excited fraction of nanostructures in the solution and follows Poisson statistics:

$$\Delta T(1\ \text{ns}) = 1 - e^{-\langle N\rangle} \quad (1)$$

where the average number of absorbed photons per nanostructure is defined as the product of the fluence and absorption cross section, $\langle N\rangle = J_0\sigma$. The number of excitons initially created per nanostructure, R_{pop}, can be estimated from the ratio of the peak photoinduced bleach to that at long delays and can be described by a modified Poisson distribution as

$$R_{pop} = \frac{\Delta T_{peak}}{\Delta T(1\ \text{ns})} = \frac{\langle N\rangle\delta\phi}{1 - e^{-\langle N\rangle}} = \frac{J_0\sigma\delta\phi}{1 - e^{-J_0\sigma}} \quad (2)$$

where σ is the absorption cross section, ϕ is the exciton quantum yield, and δ is a correction factor for single exciton decay over the temporal window.[29] Assuming a quantum yield of 1, we can fit the fluence dependence of R_{pop} in order to determine the absorption cross section. Performing these measurements as a function of relative pump−probe polarization (*i.e.*, crossed polarization *vs* parallel polarization) yields different absorption cross sections for each polarization, which can be used to calculate the absorption anisotropy. This methodology provides a unique measurement of the degree of absorption anisotropy for a randomly oriented ensemble of nanostructures.

In spite of overwhelming acceptance,[30] the assumption that ΔT grows linearly with the number of excitons created per nanostructure has recently been challenged.[31] However, we experimentally confirm the linearity of ΔT_{peak} with fluence in our nanostructure ensembles; see Supporting Information for details. Consider photoexcitation of excitons and biexcitons; clearly if biexcitons contribute more than twice the photobleaching seen from single excitons, then ΔT_{peak} would be superlinear, which is not consistent with our observations. Further, deviations in the ratio of the biexciton photobleaching (ΔT_{XX}) to single exciton photobleaching (ΔT_X) from its ideal value of 2 can easily be explained by the presence of single exciton decay. If the single exciton lifetime is ∼1−10 ns, either intrinsically or due to trapping mechanisms, then eq 1 no longer strictly holds because some excitons have decayed over the temporal window. This leads to the inclusion of δ in eq 2. For $\delta > 1$, the ratio of the biexciton to single exciton ΔT will be larger than 2. This is not due to any intrinsic nonlinearity in the material, but a failure of the assumption that the single exciton lifetime is so much longer than our temporal window that the single exciton population should experience negligible decay. As eq 2 accounts for the finite exciton lifetime, such effects will not influence our estimation of the absorption cross section.

Anisotropy Measurements of Nanorods. We measured the time-dependent photoinduced bleach dynamics at the band edge energy as a function of fluence for PbSe nanorods of aspect ratio 1 to 9 for different relative pump−probe polarizations. For specific nanorod dimensions please refer to the Supporting Information. As expected we observe more photoinduced bleaching when the pump and probe have the same polarizations (*i.e.*, parallel polarizations) than when the

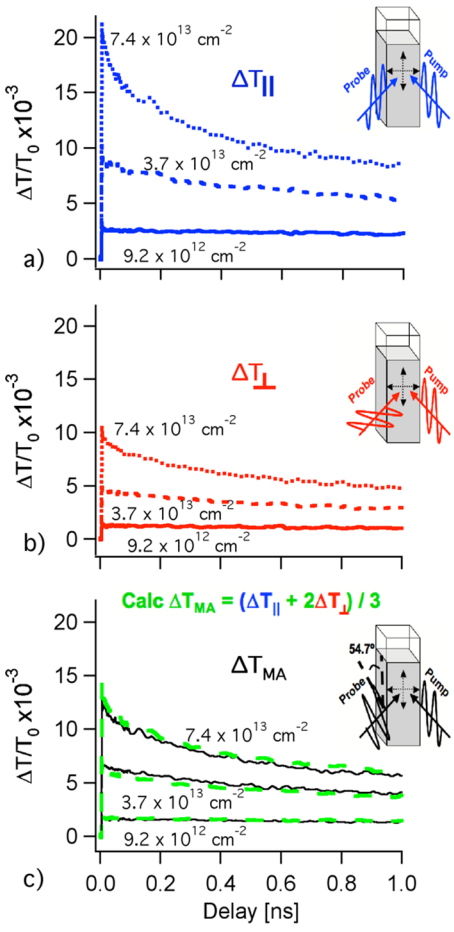

Figure 1. Time-dependent photoinduced bleach dynamics for the $1S_e-1S_h$ transition for a solution of PbSe nanorods with aspect ratio 7 ± 2 for different fluences (a) measured with parallel (blue) and (b) perpendicular (red) relative pump−probe polarizations. (c) Time-dependent photoinduced bleach dynamics for different fluences measured with probe polarization set to magic angle (black) compared to that calculated (green) from the curves in (a) and (b) using eq 3. Insets show schematic diagrams of the pump and probe polarizations incident on the cuvette containing the PbSe nanorod solution.

polarizations are perpendicular to each other (*i.e.*, crossed polarizations), Figure 1. Though the nanorods are randomly oriented in solution, the pump beam selects a subensemble of the rods that have the largest projection of their transition dipole moment in the plane of the pump electric field, Figure 2. This polarization selectivity is a consequence of the natural dichroism of nanorods; the absorbance of any given nanorod depends on the polarization of the incident light. As the excited states of nanorods are thought to be one-dimensional excitons,[17] it is equivalent to say that the pump is absorbed most strongly by the nanorods that are aligned with their axial direction parallel to the pump polarization. Those nanorods that are aligned orthogonally, *i.e.*, the radius is parallel, to the pump polarization will absorb much less of the pump beam. A probe pulse polarized parallel to the pump pulse interacts with this photoexcited subensemble and

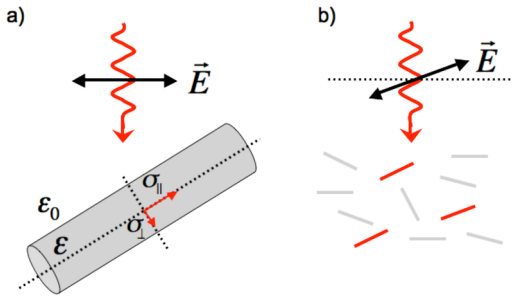

Figure 2. Schematic diagram of (a) the electric field of light interacting with a nanorod. The axial and radial absorption cross sections are drawn for reference. (b) Nanorods with their axial direction parallel to an optical electric field absorb the light most strongly (red), yielding a photoselected subpopulation with a preferred orientation.

experiences less absorption, *i.e.*, strong bleaching, due to state filling. It is the relative polarization of the probe measured with respect to the pump that matters in these measurements. This is analogous to the polarization memory effect,[21] where polarized pump excitation selects a subensemble that subsequently emits light preferentially polarized parallel to the incident pump polarization. On the other hand, a perpendicularly polarized probe is primarily absorbed by nanorods that absorbed very little pump and thus experiences less bleaching. We implicitly assume that the time delay between pump and probe pulses is insufficient for the nanorods to rotate and randomize their orientation.

Pump−probe spectroscopy is often performed at the so-called magic angle[32] to minimize the effects of delay-dependent anisotropy, which can occur if the nanorods rotate during the 1 ns temporal window. The magic angle photoinduced bleach measurements, $\Delta T_{MA}(\tau)$, in Figure 1c match those calculated from the parallel ($\Delta T_\parallel(\tau)$) and perpendicular ($\Delta T_\perp(\tau)$) cases using[33]

$$\Delta T_{MA}(\tau) = \frac{1}{3}(\Delta T_\parallel(\tau) + 2\Delta T_\perp(\tau)) \qquad (3)$$

This implies that the measured $\Delta T_\parallel$ and $\Delta T_\perp$ are free of contamination by light with orthogonal polarization. Magic angle measurements are more heavily weighted toward the case of perpendicular polarizations. This implies that previous absorption cross sections extracted from MEG measurements[14] that were performed with magic angle polarization underestimate the strong optical absorption in nanorods. The increase in the absorption of nanorods compared to nanocrystals would also be underestimated, masking a potential advantage that nanorods possess. In such studies, the reported absorption cross sections are best thought of as averages weighted more heavily toward the case of perpendicular polarizations.

Experimentally we observe that $\Delta T_\parallel \approx 2\Delta T_\perp$ for the photoinduced bleach dynamics transients for PbSe nanorods, Figure 1a, while they show no appreciable

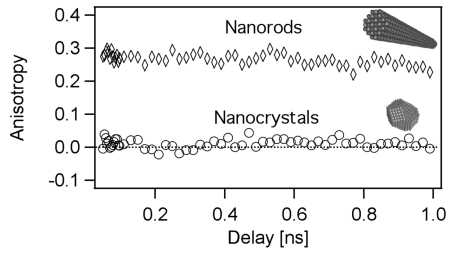

Figure 3. Comparison of the time-dependent polarization anisotropy observed in PbSe nanorods (diamonds) and nanocrystals (circles). Symbols are shown every 10 data points.

polarization dependence for nanocrystals. The time-dependent anisotropy, $\rho(\tau)$, can be calculated from these transients. It is often used to gain information about changes in the orientation of anisotropic structures or transition dipole moments. For a given pump fluence, we calculate the quantity

$$\rho(\tau) = \frac{\Delta T_{\parallel}(\tau) - \Delta T_{\perp}(\tau)}{\Delta T_{\parallel}(\tau) + 2\Delta T_{\perp}(\tau)} \quad (4)$$

For low fluences, where the contribution of sequential absorption is small, we observe polarization anisotropy that is constant over the measured temporal window, Figure 3. This rules out the possibility of rotational effects influencing our measurements here, demonstrating the validity of our implicit initial assumption.

Fluence-dependent measurements were conducted to determine the absorption cross section for each relative pump–probe polarization using eq 2. R_{pop} shows different fluence dependencies for the different probe polarizations used, Figure 4a. This is due to the different projections of the excited nanorod axes onto the plane of the probe electric field. The degree of alignment between the excited nanorods and the probe polarization changes the amount of bleaching and thus our perceived absorption cross section at the pump wavelength. For example, a probe beam polarized perpendicularly to the pump will interact with, on average, more nanorods that did not absorb pump photons and will experience less bleaching, effectively indicating to the observer that the absorption cross section is low. So the relative polarization of the probe measured with respect to the pump determines the observed absorption cross section, which is maximum for parallel relative pump–probe polarizations. If instead, the measured R_{pop} values are shown as a function of $\langle N \rangle = J_0\sigma$, we see that there is good agreement between the measurements performed with different probe polarizations, Figure 4b. This shows that the observed absorption cross section is the difference between these two measurements. In fact, the dynamics observed at $\langle N \rangle \approx 1.35$ are nearly identical for each probe polarization; see Supporting Information. A global triexponential fit to the fluence-dependent dynamics data[34] yields

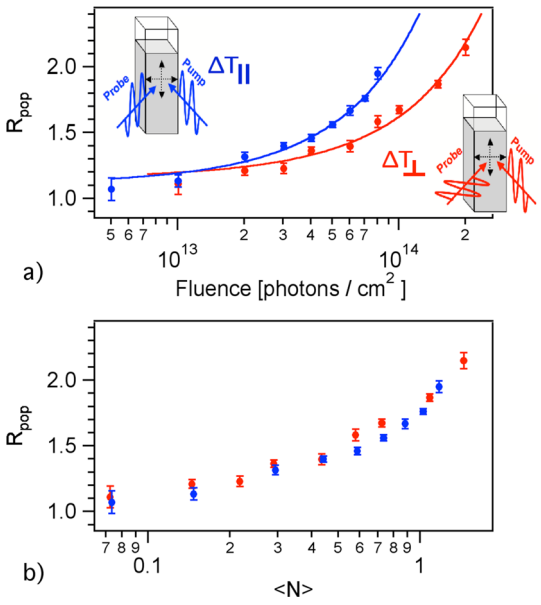

Figure 4. Comparison of the ratio of multiexciton to exciton population in PbSe nanorods as a function of (a) pump fluence and (b) average absorbed photons per nanostructure for parallel (blue) and perpendicular (red) relative pump–probe polarization.

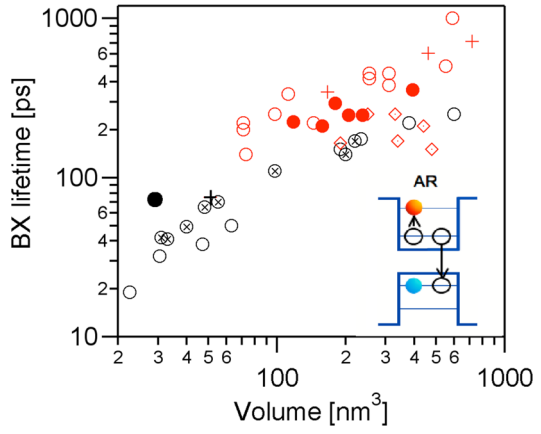

Figure 5. AR-limited biexciton (BX) lifetime as a function of nanostructure volume for PbSe nanocrystals (black) and nanorods (red). Measurements from this text (filled circles), Aerts *et al.*[35] (plus signs), Padilha *et al.*[28] (open circles), Yang *et al.*[13] (diamonds), and Beard *et al.*[36] (circles with ×) are compared. Inset shows schematic energy diagram of AR process.

an AR-limited biexciton lifetime of 263 ps for aspect ratio 7 ± 2 (~240 nm^3) nanorods, in agreement with recent AR measurements,[13,28,35] Figure 5. This observation of no change in exciton dynamics for the different polarization states indicates that neither the nanorods nor their dipole moments reorient over our 1 ns temporal window, which is consistent with the time-dependent anisotropy measurements. We conclude that dynamics measurements like those here or of AR or MEG in PbSe nanorods are not influenced by dipole reorientation, which would produce delay-dependent anisotropy.

Using eq 2, we are able to determine the absorption cross sections for parallel and perpendicular relative pump−probe polarizations in PbSe nanorods. For a randomly oriented ensemble of nanorods with an aspect ratio of 7 ± 2, the measured absorption cross section is (7.2 ± 0.4) × 10^{-15} cm^2 for perpendicular and (12.2 ± 0.7) × 10^{-15} cm^2 for parallel relative pump−probe polarizations. Given a nanorod volume of ∼240 nm^3, the absorption cross section for perpendicular relative pump−probe polarizations is roughly the same as we would expect from a nanocrystal of similar volume. However, the absorption cross section for parallel relative pump−probe polarizations is ∼1.7 times that value.

Anisotropy Measurements of Nanocrystals. We also measured the photoinduced bleach dynamics in PbSe nanocrystals as a function of relative pump−probe polarization. The nanocrystal volume was ∼29 nm^3. For a given pump fluence we observe nearly identical dynamics for both parallel and perpendicular relative pump−probe polarizations. Thus $\rho(\tau) = 0$, Figure 3, as expected for spherically symmetric nanocrystals that exhibit isotropic absorption. Fluence-dependent measurements of R_{pop} show identical curves for both parallel and perpendicular relative pump−probe polarizations, Figure 6, which indicates the same observed absorption cross section for both measurements. The measured absorption cross section is (9 ± 1) × 10^{-16} cm^2 for perpendicular and (8.6 ± 0.9) × 10^{-16} cm^2 for parallel relative pump−probe polarizations. These measurements are all consistent with isotropic absorption in PbSe nanocrystals.

Aspect Ratio Dependence of Anisotropy. We explored the nanorod aspect ratio dependence of the absorption cross section measured for parallel and perpendicular polarizations. The degree of absorption anisotropy is parametrized similarly to eq 4 as

$$\rho = \frac{\sigma_{\parallel} - \sigma_{\perp}}{\sigma_{\parallel} + 2\sigma_{\perp}} \quad (5)$$

For nanocrystals, which have an aspect ratio of 1, we observe nearly identical absorption cross sections for each polarization, which yields $\rho = 0$. However, as we have shown, elongated nanorods show a pronounced difference between the absorption cross sections measured for parallel and perpendicular relative polarizations. The anisotropy increases as the aspect ratio increases from 1 to 4 and remains relatively constant for longer nanorods, Figure 7. The trend seen here is similar to that recently observed for bulk-like short-wavelength absorption in aspect ratio 2−5 CdSe nanorods under the influence of an external ac field.[37] For aspect ratios >4, the absorption cross section for parallel polarizations is 1.8 ± 0.3 times that observed for perpendicular polarizations, which corresponds to an average anisotropy of 0.21 ± 0.06.

It should be noted that eq 5 is often seen in the literature[22−25,27] without the 2 in the denominator. Strictly speaking, that quantity is referred to as polarization,[18] while the quantity in Figure 7, calculated using eq 5, is referred to as anisotropy.[26] The former is more commonly used to describe fluorescence measurements. For comparison, the degree of polarization of the absorption as a function of nanorod aspect ratio is found in the Supporting Information.

There are two possible sources for the anisotropic absorption observed in these nanorods: dielectric contrast and quantum confinement. In the case of dielectric contrast, differences in the dielectric constants of the nanorod and the surrounding medium induce a depolarization field that, due to the anisotropic shape, more strongly attenuates the internal electric field for light polarized perpendicular to the axial direction of the rod.[21] The result is that the probability of optical transitions is larger for light polarized parallel to the axial direction. Quantum confinement may cause band mixing that modifies the optical selection rules,[17,38] altering the polarization selectivity of interband transitions. This effect has been described in detail in III−V semiconductors[39,40] and may be expected since our nanorods are ∼3−4 nm in diameter and the Bohr radius for bulk PbSe is ∼46 nm, which puts them in the strong quantum confinement regime.

As dielectric contrast is typically dominant for nanowires, we attempt to describe our nanorod results using this classical electrodynamics effect. We treat the

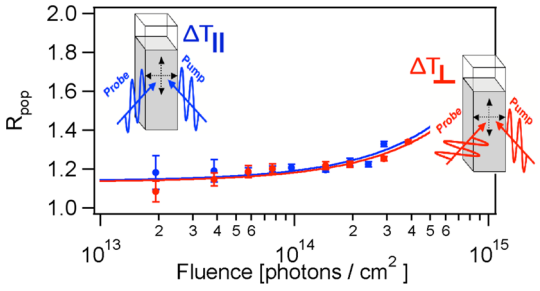

Figure 6. Comparison of the ratio of multiexciton to exciton population in PbSe nanocrystals as a function of pump fluence for parallel (blue) and perpendicular (red) relative pump−probe polarization.

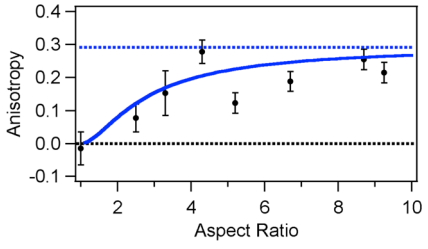

Figure 7. Dependence of the absorption anisotropy on aspect ratio. The solid blue line corresponds to the calculated anisotropy for PbSe nanorods using eqs 6 and 12. The dashed blue line corresponds to the calculated anisotropy for PbSe nanowires using eqs 8 and 12

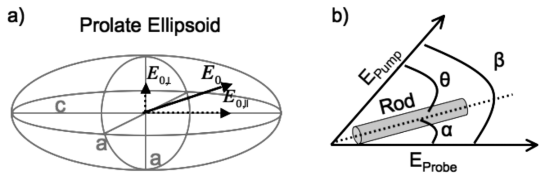

Figure 8. (a) Geometry of a prolate ellipsoidal nanorod used for eq 7, where the axial and radial field components of an applied external field are shown. (b) Geometry of our pump−probe experiment used to derive eqs 10 and 11

nanorods as prolate ellipsoids, Figure 8a, as it is done in Maxwell−Garnett effective medium theory. Dielectric contrast gives rise to a depolarization field that attenuates an applied field inside the nanostructures, producing a so-called "local field". Solving Laplace's equation for the asymmetric ellipsoidal geometry, the local field is expressed as[41]

$$E_{||,\perp} = \frac{\varepsilon_m}{\varepsilon_m + (\varepsilon - \varepsilon_m)n_{||,\perp}} E_{0||,\perp} \tag{6}$$

where $E_{0||}$ and $E_{0\perp}$ are the axial and radial projections of the incident field E_0, ε is the dielectric constant of the nanorod, and ε_m is the dielectric constant of the surrounding medium. The expression in eq 6 is equivalent to the local field factor expressions in Hyun *et al.*[42] The depolarization factors,[43] $n_{||,\perp}$, depend on the semimajor axes (a, c) of the ellipsoid as

$$\begin{aligned} n_{||} &= \frac{1-e^2}{2e^3}\left(\ln\left(\frac{1+e}{1-e}\right) - 2e\right) \\ n_{\perp} &= \frac{1-n_{||}}{2} \\ e &= \sqrt{1-a^2/c^2} \end{aligned} \tag{7}$$

Equation 7 shows that electric fields parallel to the nanorod axis are screened less while fields perpendicular to the nanorod axis are screened more than incident fields in nanocrystals; see the Supporting Information for details. Combining eqs 6 and 7, we see that the amount of attenuation that the electric field experiences depends on the aspect ratio (c/a) of the nanorods. This differs from the case of nanowires where the local field is independent of the wire dimensions,[21]

$$\begin{aligned} E_{||} &= E_{0,||} \\ E_{\perp} &= \frac{2\varepsilon_m}{\varepsilon + \varepsilon_m} E_{0,\perp} \end{aligned} \tag{8}$$

Similarly, this differs from the case of spherical nanocrystals, where the local field is isotropic due to the symmetric shape,

$$E = \frac{3\varepsilon_m}{\varepsilon + 2\varepsilon_m} E_0 \tag{9}$$

It should be pointed out that treating the nanorods as prolate ellipsoids is an approximation that is employed because the depolarization factors for a cylinder cannot be expressed in closed form. However, numerical models show that the error in approximating cylindrical rods as prolate ellipsoids is small.[44]

For our absorption anisotropy measurement we consider the light intensity, $I \propto E_\perp{}^2 + E_{||}{}^2$, in the nanorod. Given the geometry in Figure 8b, which exploits the azimuthal symmetry of the nanorods, we find that the intensity of the absorbed pump is[24]

$$I_{pump} = E_\perp{}^2 \sin^2(\beta - \alpha) + E_{||}{}^2 \cos^2(\beta - \alpha) \tag{10}$$

We must also consider the intensity of the absorbed probe,

$$I_{probe} = E_\perp{}^2 \sin^2(\alpha) + E_{||}{}^2 \cos^2(\alpha) \tag{11}$$

As pump−probe spectroscopy is a type of nonlinear spectroscopy, we take the product and consider the cases of parallel ($\beta = 0°$) and perpendicular ($\beta = 90°$) relative pump−probe polarizations. The resulting angle averaged intensities are

$$\begin{aligned} I_{||} &= I(\beta = 0°) = \frac{\pi}{4} E_\perp{}^2 E_{||}{}^2 + \frac{3\pi}{8} E_\perp{}^4 + \frac{3\pi}{8} E_{||}{}^4 \\ I_{\perp} &= I(\beta = 90°) = \frac{3\pi}{4} E_\perp{}^2 E_{||}{}^2 + \frac{\pi}{8} E_\perp{}^4 + \frac{\pi}{8} E_{||}{}^4 \end{aligned} \tag{12}$$

We can compute the anisotropy similar to eq 5 as

$$\rho = \frac{I_{||} - I_\perp}{I_{||} + 2I_\perp} \tag{13}$$

which will depend on aspect ratio for the case of nanorods.

We compute the expected anisotropy using eqs 12 and 13, taking the TCE dielectric constant to be 3.4 and assuming the PbSe nanorod's dielectric constant is the same as the PbSe bulk dielectric constant of 22.8.[45] We see good agreement between the experimental and calculated absorption anisotropy for a random ensemble of PbSe nanorods, Figure 7. For long nanorods, observed and calculated anisotropy saturate to nearly the value expected for nanowires. This suggests that, in terms of absorption anisotropy, nanorods behave as one-dimensional semiconductors for aspect ratios larger than roughly 4. Very recent measurements of the transition from cubic to bimolecular exciton recombination in PbSe nanorods show a transition of the excited state from uncorrelated charges to 1D excitons in the neighborhood of aspect ratio 6 ± 1,[35] which seems reasonably consistent with our observations of 1D excitonic behavior for aspect ratios > 4.

We can assess any enhancement in absorption in nanorods by normalizing the measured nanorod absorption cross sections to those measured for nanocrystals and assuming the absorption cross section depends linearly on volume. We find that, for aspect ratios > 4, on average the absorption cross section for perpendicular relative pump−probe polarizations in nanorods is 1.0 ± 0.2 times that measured for nanocrystals of the same volume. For parallel relative pump−probe polarizations, the volume-normalized

ratio of nanorod and nanocrystal absorption cross sections is 1.8 ± 0.6. This shows that, similar to isolated CdSe nanowires where this ratio is as large as 11,[27] randomly oriented PbSe nanorods demonstrate enhanced absorption compared to nanocrystals.

It should be pointed out that the absorption cross sections reported here are affected by orientational averaging over the randomly aligned ensemble. Using the model in eq 10, we can estimate the anisotropy of the absorption process in aligned or single nanorods, Figure 9a. For aspect ratio 7 PbSe nanorods in air we arrive at a single nanorod absorption anisotropy of 0.93, which corresponds to a 43× larger absorption cross section for light polarized parallel to the rod than for light polarized perpendicularly. The volume-normalized ratio of single nanorod and nanocrystal absorption can be estimated by the ratio of the local field factors squared for nanorods, in eq 6, and nanocrystals, in eq 9.[27] This estimate is free of orientational averaging and represents what would be expected from absorption anisotropy measurements on aligned nanorods or an individual nanorod. Owing to the large dielectric contrast, aspect ratio 7 PbSe nanorods in air will show volume-normalized absorption cross sections 22 times larger than PbSe nanocrystals. The full aspect ratio dependence is shown in Figure 9b. By the same logic, PbSe nanowires are expected to have volume-normalized absorption 68× larger than nanocrystals. This is a factor of 6 larger than the same effect in CdSe nanowires. Such enhanced absorption could be exploited by optoelectronic devices utilizing aligned nanorods.

The agreement between our measured and calculated anisotropy shows that dielectric contrast is sufficient to describe the absorption anisotropy in the PbSe nanorods measured here, without invoking quantum mechanics despite the nanorod dimensions that place them within the strong quantum confinement regime. This implies that the optoelectronic properties of nanorods may be influenced by the dielectric constant of the surrounding medium. Indeed, the degree of absorption anisotropy has been observed to decrease for CdSe nanowires embedded in poly(methyl methacrylate) compared to those in air.[46] The band gap energy depends on the exciton binding energy, which is enhanced due to image forces that arise from dielectric contrast.[47] However, changes in electron and hole self-interaction is thought to compensate for changes in exciton binding energy.[17] Therefore, the band gap may be independent of the dielectric constant of the surrounding medium. PbSe nanorods have shown aspect ratio dependent splitting of the far-infrared Fröhlich modes due to the polarization sensitivity of local field factors that results from shape anisotropy.[42] The degree of splitting will depend on the dielectric contrast. Lastly, MEG and Auger recombination both depend on Coulombic interaction.[48] The observed enhancement of MEG in nanorods[14,16] is thought to be a direct result of enhanced Coulombic interaction due to reduced screening of the electric field arising from dielectric contrast. It is therefore possible that MEG may also depend on the degree of dielectric contrast. The observed increase in MEG in PbSe nanorods compared to nanocrystals as the aspect ratio increases[28] from 2 to 4 may be related to the dependence of the electric field attenuation on aspect ratio that is described by the local field factors in eqs 6 and 7 and observed here in the absorption anisotropy in Figure 6.

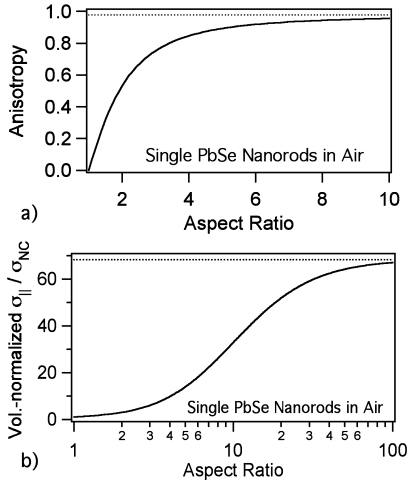

Figure 9. (a) Aspect ratio dependence of absorption anisotropy in PbSe nanorods (solid) and nanowires (dotted) from eq 10. (b) Aspect ratio dependence of the volume-normalized ratio of PbSe nanorod to nanocrystal band-edge absorption cross section, calculated from the ratio of the square of the local field factors in eq 6 and eq 9. The dotted line is the value expected for nanowires, based on the local field factors in eq 8.

While quantum confinement may also contribute to absorption anisotropy in these nanostructures, this effect is either overwhelmed by the contribution from dielectric contrast or otherwise masked by our experimental conditions. This is surprising, as the nanorod radii are more than an order of magnitude smaller than the Bohr radius (see Supporting Information for nanorod dimensions), placing them in the strong confinement regime. Recent single-nanowire measurements[25] of CdSe have observed contributions from quantum confinement to the anisotropy that may be masked in ensemble measurements. Recent photoluminescence excitation spectra and transient aborption measurements of CdSe nanorods[26] also show these quantum confinement effects, which are characterized by a wavelength dependence of the anisotropy. In both studies, the anisotropy peaks near the band edge, which is where dielectric contrast will dominate due to the axial directionality of the transition dipole. For states above the band edge, the degree of radial projection of the transition dipole becomes significant and should be taken into account.[26,49]

CONCLUSION

We have presented a means of measuring absorption anisotropy in randomly oriented solution ensembles of nanostructures that exploits the polarization memory effect *via* pump−probe spectroscopy. This technique is applied to PbSe nanostructures, where we observe isotropic absorption in nanocrystals and anisotropic absorption in nanorods. We observe an increase in anisotropy as zero-dimensional nanocrystals are elongated into quasi one-dimensional nanorods, which saturates to the value expected for one-dimensional nanowires for aspect ratios higher than 4. On the basis of our ensemble measurements, we predict that the volume-normalized absorption cross section will be 22 times larger for light polarized parallel to the rod axis of an individual aspect ratio 7 PbSe nanorod than in nanocrystals, which demonstrates an advantage to utilizing aligned nanorods in optoelectronic devices. The aspect ratio dependence of the absorption anisotropy can be described classically by the effects of dielectric contrast alone, without accounting for the influence of quantum confinement. These results imply that the dielectric constant of the surrounding medium can be used to manipulate the optoelectronic properties of nanorods, including polarized absorption and emission, phonon modes, MEG efficiency, and Auger recombination rate.

METHODS

Materials. Standard Schlenk-line techniques were used unless otherwise noted. Lead(II) oxide (PbO, 99.999%), 1-octadecene (90%), oleic acid (90%), tris(diethylamino)phosphine (97%), trioctylphosphine (90%), and selenium powder (99.5%, 100 mesh) were purchased from Sigma-Aldrich. Hexanes (98.5%) and ethanol (200 proof) were purchased from commercial sources. PbO, trioctylphosphine, Se, hexanes, and ethanol were used without further purification. Oleic acid and 1-octadecene were dried by heating them to 110 °C under vacuum for 2 h and then placing them over activated 3 Å molecular sieves in a glovebox. Tris(diethylamino)phosphine was purified by first heating under Ar to 225 °C for 2 to 3 h to decompose minor impurities, signified by the onset of a yellow color, followed by vacuum distillation under a dynamic vacuum of ∼200 mTorr at 65 to 77 °C.

PbSe Nanorod Synthesis. PbSe nanorods of varying aspect ratio were synthesized using the method described in Boercker *et al.*[50] This is a modification of the method described in Koh *et al.*[51] in order to purposefully control the nanorod aspect ratio. The longer aspect ratio nanorods were made by carefully drying all the precursors to remove any trace water contamination. The nanorod aspect ratio was lowered by intentionally adding water to the dry reaction, with more water creating lower aspect ratios. To synthesize PbSe nanorods in the absence of water, dried Pb-oleate isolated as described below (0.77 g; 1 mmol), dried oleic acid (0.37 mL; 1.2 mmol), and 5 mL of dried 1-octadecene were mixed under Ar and heated to 150 °C. Next, 3 mL of purified tris(diethylamino)phosphine was mixed with Se (0.237 g; 3 mmol) and loaded into a syringe. This solution was then injected into the Pb-oleate solution, which caused the temperature to drop to ∼130 °C. The reaction was allowed to continue for 2 min, during which time the temperature rose to ∼135 °C. The reaction became a dark brown color after ∼80 s. After 2 min, the reaction was cooled to room temperature using a liquid nitrogen bath. The nanorods were isolated from the unreacted precursors and byproducts by adding ∼0.5 mL of hexanes and ∼8 mL of ethanol and centrifuging at 4 kprm for 4 min. This process was performed in air. The product formed a black solid at the bottom of the vial, which was separated by decanting. This purification procedure was repeated using ∼1 mL of hexanes and ∼5 mL of ethanol. The nanorods were immediately transferred into an Ar-filled glovebox for storage.

When water was intentionally added to the reaction in order to decrease the nanorod aspect ratio, the same method described above was followed except small amounts of water were added to the Pb-oleate, oleic acid, and 1-octadecene solution before heating. The amounts of water added and the resulting dimensions are given in the Supporting Information.

Synthesis of Pb-oleate. Typically, 4.4 g (20 mmol) of PbO and 19 mL of oleic acid (60 mmol) were heated to 110 °C under vacuum for 2 h. Once the solution was colorless, it was placed in two vials while it was still above room temperature. The viscous solution of Pb-oleate and oleic acid was allowed to cool to room temperature overnight, and the mixture became a fluffy, sticky, white solid. The extra oleic acid was removed by washing the solid with acetone, forming a milky white suspension. Next, the solution was centrifuged at 4 krpm for 3 min, which caused the solid Pb-oleate to separate from the solution and deposit on the bottom of the vial, leaving the oleic acid in the acetone. This acetone-cleaning step was repeated eight times in order to ensure that all the oleic acid was removed. The Pb-oleate was then placed in a vacuum oven at room temperature overnight in order to remove any remaining acetone and water. Finally, the vacuum oven was backfilled with Ar, and the white powdery Pb-oleate was stored in a glovebox.

Synthesis of PbSe Nanocrystals. PbSe nanocrystals were synthesized following the method developed by Yu *et al.*[52] Pb-oleate (0.77 g; 1 mmol, synthesized as described above), oleic acid (0.08 g; 0.28 mmol, not dried), and 1-octadecene (3.9 g; 15 mmol, not dried) were combined and heated under vacuum to 110 °C for 30 min and then heated to 130 °C under Ar. Next, room-temperature Se (0.16g, 2 mmol) was mixed with trioctylphosphine (2 mL) and then injected into the Pb-oleate mixture. The solution turned dark brown after ∼60 s and was cooled to room temperature after 3 min using liquid nitrogen. The byproducts and unreacted precursors were removed from the nanocrystals by adding ∼1 mL of hexanes and ∼10 mL of ethanol and then centrifuging at 4 krpm for 4 min; this was done in air. The nanocrystals formed a dark solid at the bottom of the vial, which was isolated by decanting the solution. This cleaning process was performed twice, and then the nanocrystals were stored in an Ar-filled glovebox.

Sample Preparation. Solution samples were prepared in an Ar-filled glovebag using freeze−pump−thawed tetrachloroethylene. The solution was prepared in a stirring cuvette, which was closed with a PTFE cap and sealed with Parafilm tape. Absorbance spectroscopy was performed using a Lambda 750 spectrophotometer to determine the $1S_e-1S_h$ excitonic absorption wavelength; for details see the Supporting Information. The optical densities were between 0.1 and 0.3 at the $1S_e-1S_h$ transition. The nanostructure dimensions were determined from transmission electron microscopy images.

Pump−Probe Experiments. We utilize a standard two-color sub-picosecond resolution pump−probe experimental setup, which has been detailed elsewhere.[53] In brief, a 1 kHz Clark-MXR CPA Ti:sapphire amplifier was used to pump a ∼150 fs Clark-MXR infrared OPA, which was set to the band edge absorption feature; see Supporting Information for the wavelengths corresponding to the band edge transition for each solution of nanorods. Degenerate pump−probe experiments were used to determine the absorption cross section at the $1S_e-1S_h$ transition using eq 2 and the method outlined in the text. In our previous studies, the probe polarization was set to the

magic angle[32] (54.7°) with respect to the pump polarization using a half-wave plate to avoid any potential artifacts due to rotation effects.[33] Here, a half-wave plate and Glan–Taylor polarizing beam cube were used to set the polarization state of the probe beam, either parallel or perpendicular to the pump polarization. The polarization state of the pump was p-polarized and was purified with another Glan–Taylor polarizer. A balanced InGaAs photoreceiver was used to detect the probe beam and a reference beam transmitted through free space. Lock-in detection of the pump–probe delay dependent photoinduced bleach dynamics was employed.

Conflict of Interest: The authors declare no competing financial interest.

Acknowledgment. The Office of Naval Research (ONR) is gratefully acknowledged for their financial support of this work. D.P. acknowledges the Nation Research Council research associates program.

Supporting Information Available: Details concerning the linearity of the pump–probe signal, the independence of measured exciton dynamics on polarization, and the nanorod depolarization factors, differences between polarization and anisotropy, derivation of eq 12, nanorod synthesis, dimensions, and TEM images. This material is available free of charge *via* the Internet at http://pubs.acs.org.

REFERENCES AND NOTES

1. Sargent, E. H. Infrared Photovoltaics Made By Solution Processing. *Nat. Photonics* **2009**, *3*, 325–331.
2. Semonin, O. E.; Luther, J. M.; Choi, S.; Chen, H.-Y.; Gao, J.; Nozik, A. J.; Beard, M. C. Peak External Photocurrent Quantum Efficiency Exceeding 100% via MEG in a Quantum Dot Solar Cell. *Science* **2011**, *334*, 1530–1533.
3. Etgar, L.; Yanover, D.; Capek, R. K.; Vaxenburg, R.; Xue, Z.; Liu, B.; Nazeeruddin, M. K.; Lifshitz, E.; Grätzel, M. Core/Shell PbSe/PbS QDs TiO_2 Heterojunction Solar Cell. *Adv. Funct. Mater.* **2013**, *23*, 2736–2741.
4. Yoon, W.; Boercker, J. E.; Lumb, M. P.; Placencia, D.; Foos, E. E.; Tischler, J. G. Enhanced Open-Circuit Voltage of PbS Nanocrystal Quantum Dot Solar Cells. *Sci. Rep.* **2013**, *3*, 2225.
5. Ma, W.; Luther, J. M.; Zheng, H.; Wu, Y.; Alivisatos, A. P. Photovoltaic Devices Employing Ternary PbS_xSe_{1-x} Nanocrystals. *Nano Lett.* **2009**, *9*, 1699–1703.
6. Sukhovatkin, V.; Hinds, S.; Brzozowski, L.; Sargent, E. H. Colloidal Quantum-Dot Photodetectors Exploiting Multiexciton Generation. *Science* **2009**, *324*, 1542–1544.
7. Caruge, J. M.; Halpert, J. E.; Wood, V.; Bulovic, V.; Bawendi, M. G. Colloidal Quantum-Dot Light-Emitting Diodes with Metal-Oxide Charge Transport Layers. *Nat. Photonics* **2008**, *2*, 247–250.
8. Sun, L.; Choi, J. J.; Stachnik, D.; Bartnik, A. C.; Hyun, B.-R.; Malliaras, G. G.; Hanrath, T.; Wise, F. W. Bright Infrared Quantum-Dot Light-Emitting Diodes through Inter-Dot Spacing Control. *Nat. Nanotechnol.* **2013**, *7*, 369–373.
9. Klimov, V. I.; Mikhailovsky, A. A.; Xu, S.; Malko, A.; Hollingsworth, J. A.; Leatherdale, C. A.; Eisler, H.-J.; Bawendi, M. G. Optical Gain and Stimulated Emission in Nanocrystal Quantum Dots. *Science* **2000**, *290*, 314–317.
10. Pietryga, J. M.; Werder, D. J.; Williams, D. J.; Casson, J. L.; Schaller, R. D.; Klimov, V. I.; Hollinsworth, J. A. Utilizing the Lability of Lead Selenide to Produce Heterostructured Nanocrystals with Bright, Stable Infrared Emission. *J. Am. Chem. Soc.* **2008**, *130*, 4879–4885.
11. Medintz, I. L.; Uyeda, H. T.; Goldman, E. R.; Mattoussi, H. Quantum Dot Bioconjugates for Imaging, Labelling and Sensing. *Nat. Mater.* **2005**, *4*, 435–446.
12. Htoon, H.; Hollingsworth, J. A.; Dickerson, R.; Klimov, V. I. Effects of Zero- to One-Dimensional Transformation on Multiparticle Auger Recombination in Semiconductor Quantum Rods. *Phys. Rev. Lett.* **2003**, *91*, 227401.
13. Yang, J.; Hyun, B.-R.; Basile, A. J.; Wise, F. W. Exciton Relaxation in PbSe Nanorods. *ACS Nano* **2012**, *6*, 8120–8127.
14. Cunningham, P. D.; Boercker, J. E.; Foos, E. E.; Lumb, M. P.; Smith, A. R.; Tischler, J. G.; Melinger, J. S. Enhanced Multiple Exciton Generation in Quasi-One-Dimensional Semiconductors. *Nano Lett.* **2011**, *11*, 3476–3481.
15. Cunningham, P. D.; Boercker, J. E.; Foos, E. E.; Lumb, M. P.; Smith, A. R.; Tischler, J. G.; Melinger, J. S. Correction to Enhanced Multiple Exciton Generation in Quasi-One-Dimensional Semiconductors. *Nano Lett.* **2013**, *13*, 3003–3003.
16. Sandberg, R. L.; Padilha, L. A.; Qazilbash, M. M.; Bae, W. K.; Schaller, R. D.; Pietryga, J. M.; Stevens, M. J.; Baek, B.; Nam, S. W.; Klimov, V. I. Multiexciton Dynamics in Infrared-Emitting Colloidal Nanostructures Probe by a Superconducting Nanowire Single Photon Detector. *ACS Nano* **2012**, *6*, 9532–9540.
17. Bartnik, A. C.; Efros, A. L.; Koh, W.-K.; Murray, C. B.; Wise, F. W. Electronic States and Optical Properties of PbSe Nanorods and Nanowires. *Phys. Rev. B* **2010**, *82*, 195313.
18. Hu, J.; Li, L.-s.; Yang, W.; Manna, L.; Wang, L.-w.; Alivisatos, A. P. Linearly Polarized Emission from Colloidal Semiconductor Quantum Rods. *Science* **2001**, *292*, 2060–2063.
19. Wang, J.; Gudiksen, M. S.; Duan, X.; Cui, Y.; Lieber, C. M. Highly Polarized Luminescence and Photodetection from Single InP Nanowires. *Science* **2001**, *292*, 1455–1457.
20. Tischler, J. G.; Kennedy, T. A.; Glaser, E. R.; Efros, A. L.; Foos, E. E.; Boercker, J. E.; Zega, T. J.; Stroud, R. M.; Erwin, S. C. Band-Edge Excitons in PbSe Nanocrystals and Nanorods. *Phys. Rev. B* **2010**, *82*, 245303.
21. Ruda, H. E.; Shik, A. Polarization-Sensitive Optical Phenomena in Semiconducting and Metallic Nanowires. *Phys. Rev. B* **2005**, *72*, 115308.
22. Protasenko, V.; Bacinello, D.; Kuno, M. Experimental Determination of the Absorption Cross-Section and Molar Excitinction Coefficient of CdSe and CdTe Nanowires. *J. Phys. Chem. B* **2006**, *110*, 25322–25331.
23. Giblin, J.; Protasenko, V.; Kuno, M. Wavelength Sensitivity of Single Nanowire Excitation Polarization Anisotropies Explained through a Generalized Treatment of Their Linear Absorption. *ACS Nano* **2009**, *3*, 1979–1987.
24. Yu, Y.; Protasenko, V.; Jena, D.; Xing, H.; Kuno, M. Photocurrent Polarization Anisotropy of Randomly Oriented Nanowire Networks. *Nano Lett.* **2008**, *8*, 1352–1357.
25. McDonald, M.; Vietmeyer, F.; Kuno, M. Direct Measurement of Single CdSe Nanowire Exctinction Polarization Anisotropies. *J. Phys. Chem. Lett.* **2012**, *3*, 2215–2220.
26. Tice, D. B.; Weinberg, D. J.; Mathew, N.; Chang, R. P. H.; Weiss, E. A. Measurement of Wavelength-Dependent Polarization Character in the Absorption Anisotropies of Ensembles of CdSe Nanorods. *J. Phys. Chem. C* **2013**, *117*, 13289–13296.
27. Giblin, J.; Kuno, M. Nanostructure Absorption: A Comparative Study of Nanowire and Colloidal Quantum Dot Absorption Cross Sections. *J. Phys. Chem. Lett.* **2010**, *1*, 3340–3348.
28. Padilha, L. A.; Stewart, J. T.; Sandberg, R. L.; Bae, W. K.; Koh, W.-h.; Pietryga, J. M.; Klimov, V. I. Aspect Ratio Dependence of Auger Recombination and Carrier Multiplication in PbSe Nanorods. *Nano Lett.* **2013**, *13*, 1092–1099.
29. Luther, J. M.; Beard, M. C.; Song, Q.; Law, M.; Ellingson, R. J.; Nozik, A. J. Multiple Exciton Generation in Films of Electronically Coupled PbSe Quantum Dots. *Nano Lett.* **2007**, *7*, 1779–1784.
30. Klimov, V. I.; Mikhailovsky, A. A.; McBranch, D. W.; Leatherdale, C. A.; Bawendi, M. G. Quantization of Multiparticle Auger Rates in Semiconductor Quantum Dots. *Science* **2000**, *287*, 1011–1013.
31. Karki, K. J.; Ma, F.; Zheng, K.; Zidek, K.; Mousa, A.; Abdellah, M. A.; Messing, M. E.; Wallenberg, L. R.; Yartsev, A.; Pullerits, T. Multiple Exciton Generation in Nano-Crystals Revisited: Consistent Calculation of the Yield Based on Pump-Probe Spectroscopy. *Sci. Rep.* **2013**, *3*, 2287.
32. Tao, T. Time-Dependent Fluorescence Depolarization and Brownian Rotational Diffusion Coefficients of Macromolecules. *Biopolymers* **1969**, *8*, 609–632.
33. Lessing, H. E.; Von Jena, A. Separation of Rotational Diffusion and Level Kinetics in Transient Absorption Spectroscopy. *Chem. Phys. Lett.* **1976**, *42*, 213–217.

34. Ellingson, R. J.; Beard, M. C.; Johnson, J. C.; Yu, P.; Micic, O. L.; Nozik, A. J.; Shabaev, A.; Efros, A. L. Highly Efficient Multiple Exciton Generation in Colloidal PbSe and PbS Quantum Dots. *Nano Lett.* **2005**, *5*, 865–871.
35. Aerts, M.; Spoor, F. C. M.; Grozema, F. C.; Houtepen, A. J.; Schins, J. M.; Siebbeles, L. D. A. Cooling and Auger Recombination of Charges in PbSe Nanorods: Crossover from Cubic to Bimolecular Decay. *Nano Lett.* **2013**, *13*, 4380–4386.
36. Beard, M. C.; Ellingson, R. J. Multiple Exciton Generation in Semiconductor Nanocrystals: Toward Efficient Solar Energy Conversion. *Laser Photonics Rev.* **2008**, *2*, 377–399.
37. Kamal, J. S.; Gomes, R.; Hens, Z.; Karvar, M.; Neyts, K.; Compernolle, S.; Vanhaecke, F. Direct Determination of Absorption Anisotropy in Colloidal Quantum Rods. *Phys. Rev. B* **2012**, *85*, 035126.
38. Efros, A. L.; Rosen, M. The Electronic Structure of Semiconductor Nanocrystals. *Annu. Rev. Mater. Sci.* **2000**, *30*, 475–521.
39. Persson, M. P.; Xu, H. Q. Giant Polarization Anisotropy in Optical Transistions of Free-Standing InP Nanowires. *Phys. Rev. B* **2004**, *70*, 161310(R).
40. Sercel, P. C.; Vahala, K. J. Analytical Technique for Determining the Polarization Dependence of Optical Matrix Elements in Quantum Wires with Band-Coupling Effects. *Appl. Phys. Lett.* **1990**, *57*, 545–547.
41. Ruda, H. E.; Shik, A., Polarization-Sensitie Nanowire and Nanorod Optics. In *Handbook of Nanophysics*; Sattler, K. D., Ed.; CRC Press: Boca Raton, FL, 2011; Vol. 6.
42. Hyun, B.-R.; Bartnik, A. C.; Koh, W.-k.; Agladze, N. I.; Wrubel, J. P.; Sievers, A. J.; Murray, C. B.; Wise, F. W. Far-Infrared Absorption of PbSe Nanorods. *Nano Lett.* **2011**, *11*, 2786–2790.
43. Kovalev, D.; Chorin, M. B.; Diener, J.; Koch, F.; Efros, A. L.; Rosen, M.; Gippius, N. A.; Tikhodeev, S. G. Porous Si Anisotropy from Photoluminescence Polarization. *Appl. Phys. Lett.* **1995**, *67*, 1585–1587.
44. Venermo, J.; Sihvola, A. Dielectric Polarizability of Circular Cylinder. *J. Electrost.* **2005**, *63*, 101–117.
45. Zemel, J. N.; Jensen, J. D.; Schoolar, R. B. Electrical and Optical Properties of Epitaxial Films of PbS, PbSe, PbTe, and SnTe. *Phys. Rev.* **1965**, *140*, A330.
46. Lan, A.; Giblin, J.; Protasenko, V.; Kuno, M. Excitation and Photoluminescence Polarization Anisotropy of Single CdSe Nanowires. *Appl. Phys. Lett.* **2008**, *92*, 183110.
47. Shabaev, A.; Efros, A. L. 1D Exciton Spectroscopy of Semiconductor Nanorods. *Nano Lett.* **2004**, *4*, 1821–1825.
48. Shabaev, A.; Hellberg, C. S.; Efros, A. L. Efficiency of Multiexciton Generation in Colloidal Nanostructures. *Acc. Chem. Res.* **2013**, *46*, 1242–1251.
49. Hadar, I.; Hitin, G. B.; Sitt, A.; Faust, A.; Banin, U. Polarization Properties of Semicondcutor Nanorod Heterostructures: From Single Particles to the Ensemble. *J. Phys. Chem. Lett.* **2013**, *4*, 502–507.
50. Boercker, J. E.; Foos, E. E.; Placencia, D.; Tischler, J. G. Control of PbSe Nanorod Aspect Ratio by Limiting Phosphine Hydrolysis. *J. Am. Chem. Soc.* **2013**, *135*, 15071–15076.
51. Koh, W.-K.; Bartnik, A. C.; Wise, F. W.; Murray, C. B. Synthesis of Monodisperse PbSe Nanorods: A Case of Oriented Attachment. *J. Am. Chem. Soc.* **2010**, *132*, 3909–3913.
52. Yu, W. W.; Falkner, J. C.; Shih, B. S.; Colvin, V. L. Preparation and Characterization of Monodisperse PbSe Semiconductor Nanocrystals in a Noncoordinating Solvent. *Chem. Mater.* **2004**, *16*, 3318–3322.
53. Cunningham, P. D.; Boercker, J. E.; Foos, E. E.; Lumb, M. P.; Smith, A. R.; Tischler, J. G.; Melinger, J. S. In *Multiple Exciton Generation in PbSe Nanorods, Physics, Simulation, and Photonic Engineering of Photovoltaic Devices*; Freundlich, A.; Guillemoles, J.-F. F., Eds.; Proceedings of SPIE: San Francisco, CA, Jan 2012; p 825610.